Comprehensive theoretical and experimental study of near infrared absorbing copolymers based on dithienosilole

Katarzyna Brymora, Wissem Khelifi, Hussein Awada, Sylvie Blanc, Lionel Hirsch, Antoine Bousquet, Christine Lartigau-Dagron, Frédéric Castet

ARTICLE

Comprehensive theoretical and experimental study of near infrared absorbing copolymers based on dithienosilole

Received 00th January 20xx,
Accepted 00th January 20xx

DOI: 10.1039/x0xx00000x

Katarzyna Brymora,[a] Wissem Khelifi,[b] Sylvie Blanc,[b] Lionel Hirsch,[c] Antoine Bousquet,[b,*] Christine Lartigau-Dagron,[b,*] and Frédéric Castet[a,*]

In recent contributions [*Eur. Polym*. J. 2013, 49, 4176; *Macromolecules* 2019, 52, 13, 4820], we reported a series of low band gap copolymers with the objective of shifting the absorption from the visible to the near infrared range. This polymer family is based on the combination of the dithienosilole (DTS) electron rich unit with different electron-withdrawing units, namely benzothiadiazole (BT), 4,7-di(thiophen-2-yl)-2,1,3-benzothiadiazole (DTBT), diketopyrrolopyrrole (DPP) and diazapentalene (DAP). In the present report, we extend this family by designing a new copolymer alternating the DTS donor with the thienoisoindigo (TII) acceptor. The experimental characterizations are rationalized by means of DFT calculations, which provide structure−property relationships linking absorption properties of the various copolymers to the electronic structure of the ground and first excited states. To enable more complete analyses, we also carried out DFT calculations on ten supplementary copolymers based on electron rich monomers analogues to DTS, cyclopentadithiophene (CPDT) and dithienopyrrole (DTP). Electrochemical and optical properties of the DTS-TII copolymer are compared to those of copolymers incorporating BT, DTBT, DPP and DAP accepting units. We show that this new copolymer exhibits an improved near-infrared light harvesting in both solution and thin films, which makes this material of interest for a variety of optoelectronics applications.

1. Introduction

Owing to their applicability in a wide range of devices such as organic photovoltaic cells (OPV), photodetectors (OPDs) or organic field-effect transistors (OFETs), extensive research was dedicated in the last 20 years to design conjugated donor-acceptor (D-A) copolymers with high light-harvesting capabilities in the near-infrared (NIR) range.[1,2,3,4,5,6,7] D–A copolymers involve alternating electron-rich and electron-poor moieties along their conjugated backbone, which induces a stabilization of the quinoid resonance structure that results in a lowering of the optical bandgap.[8] Tuning the absorption profile of D-A copolymers can be achieved by varying the relative strengths of the D and A building blocks, strategy which has been widely employed to design materials with narrow band gap (below 1.6 eV) showing efficient absorption in the first NIR window (750-1000 nm). Recently, a new research focus turned to organic polymers absorbing in the second NIR window (1000-1350 nm), i.e. below the absorption cut-off of silicon. Such materials are of particular interest for biological applications, since second NIR wavelengths display deeper penetration in tissues.[9,10]

Plethora of electron-donating (D) units were employed for designing low band gap copolymers, such as thiophene, bithiophene, thieno[3,2-b]thiophene, carbazole, fluorene, dibenzosilole, benzodithiophene (BDT), cyclopentadithiophene (CPDT), dithienosilole (DTS), or dithienopyrrole. Among them, DTS has attracted attention owing to its ease of synthesis, photostability, as well as the possibility of introducing ethyl-hexyl side chains onto the silicon atom to increase solubility.[11,12] The DTS unit was combined with various electron-accepting moieties including (albeit non-exhaustively) pyridine and dithienylpyridine,[13] tricoordinate boron units,[14] quinoxaline,[15] thienopyrrole-4,6-dione,[16] thiazolothiazole,[17] benzothiadiazole (BT) and 4,7-di(thiophen-2-yl)-2,1,3-benzothiadiazole (DTBT),[18,19,20,21] and fluoro-benzothiadiazole.[22]

Compared to DTS-BT, some of us showed in a previous work that the addition of hexylthiophene units in DTS-DTBT induces a significant blue-shift of the low-energy band, which was attributed to a larger structural distortion of the π-conjugated backbone due to the presence of hexyl side chains.[21] More recently, we reported the synthesis and optoelectronic

[a] Institut des Sciences Moléculaires (ISM, UMR CNRS 5255), Université de Bordeaux, 351 cours de la Libération, 33405 Talence, France. frederic.castet@u-bordeaux.fr.
[b] CNRS/Université de Pau et des Pays de l'Adour/E2S UPPA, IPREM CNRS-UMR 5254 Hélioparc, 2 avenue Président Angot, 64053 Pau Cedex 9, France. antoine.bousquet@univ-pau.fr; christine.lartigau-dagron@univ-pau.fr.
[c] Univ. Bordeaux, IMS, CNRS, UMR 5218, Bordeaux INP, ENSCBP, F-33405 Talence, France.

Electronic Supplementary Information (ESI) available: [Computational: Electronic and optical properties of increasingly large oligomers and extrapolation to polymer properties; Experimental: Synthesis and NMR data of the TII monomer and DTS-TII polymer.]. See DOI: 10.1039/x0xx00000x

properties of dithienosilole-diketopyrrolopyrrole (DTS-DPP) and dithienosilole-diazapentalene (DTS-DAP) copolymers. The latter evidenced spectacular halochromic properties, with a shift of the maximum absorbance from the first to the second NIR window upon addition of Brønsted or Lewis acids.[23]

In the present work, we report the synthesis of a new copolymer combining DTS to the thienoisoindigo (TII) unit. TII recently emerged as an efficient electron-withdrawing moiety for high-performance polymers owing to the planarity of the polymer backbone induced by the strong sulfur–oxygen interactions, as well as its quinoidal nature that enables improved charge delocalization and transport.[24,25,26,27]

In this contribution, the electrochemical and optical properties of the DTS-TII copolymer are compared to those measured in the same conditions for the previously reported DTS-based copolymers, namely DTS-BT, DTS-DTBT, DTS-DPP and DTS-DAP. To fully rationalize the evolution of the absorption properties in this series, cyclic voltammetry (CV) and UV/visible (UV/vis) characterizations are complemented by quantum chemical calculations based on the Density Functional Theory (DFT). Computational chemistry provides a direct insight on the impact of chemical modifications in these structurally similar systems. The optical responses are rationalized by considering the geometrical structure of the polymers, the nature of the electron-withdrawing unit, and by analysing the electronic structure of the ground and first dipole-allowed excited electronic states. In order to establish more complete structure–property relationships, DFT calculations were also carried out on copolymers incorporating electron-rich cyclopentadithiophene (CPDT) or dithienopyrrole (DTP) units (Figure 1). These analogues to DTS, which respectively include a carbon or nitrogen bridging atom instead of silicon, are also standard electron-donating building blocks used in the design of low bandgap alternating D-A polymers.[4,6,28,29]

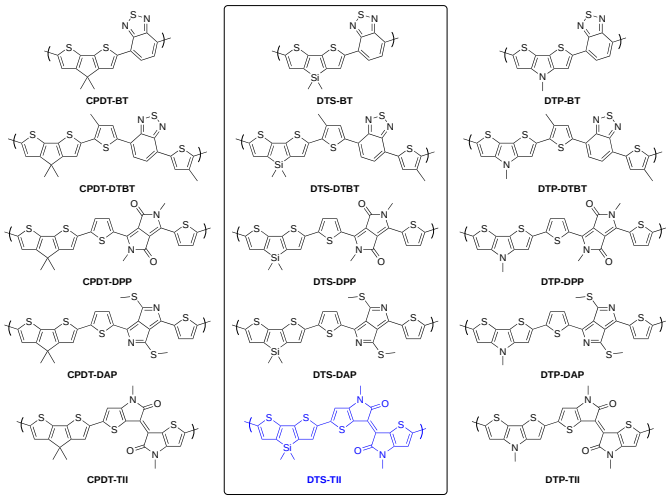

Figure 1: Chemical structure of the investigated donor-acceptor (D-A) units, with framed the structures characterized experimentally and in blue the newly synthesized DTS-TII system. Solubilizing alkyl chains present in structures characterized experimentally, namely ethyl-hexyl chains on the DTS, DPP and DAP units, hexyl chains on the thiophene groups of DTBT, as well as didodecyl chains on the TII moieties, have been replaced by methyl substituents in all calculations, as represented.

2. Experimental and computational methods

2.1 Quantum Chemical Calculations

Electronic and optical properties of copolymers have been evaluated by using the oligomer approach, in which the properties of oligomers containing an increasing number of repeating units (from n = 1 to n = 5) are first calculated, and then extrapolated to infinite polymeric chains.[30] Geometry optimizations have been carried out at the DFT level using the M06-2X exchange correlation (XC) functional[31] and the 6-311G(d) basis set. This XC functional contains 54% of Hartree−Fock exchange, and was shown to reliably describe the torsion angles and bond length alternation (BLA) of extended π-conjugated systems,[32,33] which is prerequisite for accurate predictions of optical properties. Several input geometries differing by the values of the torsion angles around single bonds have been considered for monomers and dimers to systematically sample the conformational space and identify the lowest-energy conformation. The starting geometries of increasingly large oligomers were then built by replicating this particular orientation before optimization. All oligomers up to n = 3 monomeric units were confirmed as real minima of the potential energy surface on the basis on their positive vibrational force constants.

Vertical transition energies and excited state properties of oligomers have been calculated by employing the Time-Dependent Density Functional Theory (TD-DFT) at the M06-2X/6-311G(d) level. Optical properties have been calculated both in gas phase and by including solvent effects (chloroform) using the Integral Equation Formalism of the Polarizable Continuum Model (IEFPCM).[34] In the case of monomers, the photo-induced charge transfer has been quantified by the dipole moment variation $\Delta\mu_{01}$ between the ground (S_0) and first excited (S_1) singlet states, which can be further decomposed as the product of the photo-induced charge displacement (Δq) and charge transfer distance (Δr): $\Delta\mu_{01} = \Delta q \times \Delta r$. The $S_0 \rightarrow S_1$ transition energies in the polymer limit ($\Delta \boldsymbol{E}_{\boldsymbol{01}}^{\boldsymbol{\infty}}$) have been evaluated using the fitting equation issued from the Kuhn's coupled oscillator model[35] (Electronic Supplementary Information, ESI). This procedure was demonstrated as reliable in many theoretical investigations of π-conjugated polymers including alternating D-A copolymers.[33,36,37,38,39] All calculations have been performed with the Gaussian09 package.[40]

2.2 Experimental Characterizations

Cyclic Voltammetry. A standard three-electrode electrochemical setup (AUTOLAB PGSTAT 101) consisting of a glassy carbon or a platinium disk as working electrode (2 mm diameter), a platinum foil as counter electrode, and an Ag/AgCl as reference electrode, have been used in electrochemical experiments. At the end of each experiment performed in CH_3CN/Bu_4NPF_6 (0.1 M), the standard potential of the

ferrocenium/ferrocene couple ($E_{Fc+/Fc}$) has been measured (Fig. S3.1), and all potentials have been referenced against SCE using a previous determination of $E_{Fc+/Fc}$ = 0.41 V versus SCE in CH_3CN. Polymers were drop casted from a 10 mg/mL polymer solution in chlorobenzene/Bu_4NPF_6 (0,1 M) on the working electrode. CV can give information on the oxidation and reduction potentials of materials. Indeed, HOMO and LUMO energy levels were estimated using the empirical equations: E_{HOMO} (eV) = - (Eox + 4.7) and E_{LUMO} (eV) = - (E_{red} + 4.7), where E_{ox} and E_{red} are respectively the onset potentials for oxidation and reduction waves relative to SCE, and 4.7 the factor connecting SCE to vacuum. The onset potentials have been determined by the tangent method. Only values from the first sweep on a film have been used as the film may change or be degraded during the first oxidation. The scan rate used is 0.1 $V.s^{-1}$.

Nuclear Magnetic Resonance Spectroscopy. Proton, carbon and heteronuclear multiple-bond correlation (HMBC) spectra were recorded in deuterated chloroform as a solvent using a Bruker 400 MHz spectrometer at 25 °C.

Absorption spectroscopy. The absorption spectra were recorded at room temperature with a double beam Cary 5000 spectrophotometer in steps of 1 nm in the range 400-1600 nm using a 1 cm quartz optical cell (Hellma).

2.3 Polymer synthesis

Except P(DTS-TII) reported for the first time here, the synthesis of the DTS-DTBT, DTS-BT, DTS-DPP and DTS-DAP copolymers have been detailed in our previous works.[21,23] All polymers have been synthesized using Stille polycondensation of 5,5'-bis(trimethylstannyl)-3,3'-di-n-octylsilylene-2,2'-bithiophene (DTS monomer, purchased from 1-Material and used as received) and respective dibrominated BT, DTBT, DPP, DAP and TII acceptors. In a 10 mL high pressure microwave reactor tube equipped with a sealed septum, a solution of DTS monomer (1eq) and the acceptor monomer (1eq) was taken in anhydrous chlorobenzene (2 ml) in the glovebox. To the solution, tris(dibenzylideneacetone) dipalladium(0) ($Pd_2(dba)_3$, 2 mol %), tri(o-tolyl)phosphine ($P(o\text{-}Tol)_3$, 8 mol %) have been dissolved in 3 mL of anhydrous chlorobenzene in the glovebox. Both solutions have been mixed and heated at 130°C for 6h. After cooling to room temperature, the resulting viscous liquid has been diluted in chlorobenzene and then precipitated into methanol. The solid has been filtered through a Soxhlet thimble and then subjected to Soxhlet extraction with methanol, acetone, cyclohexane, and chloroform. The chloroform fraction has been concentrated and precipitated into methanol. Finally, the precipitant has been filtered and dried under high vacuum to afford the different polymers. The general synthetic strategy is illustrated in Figure 2 in the case of P(DTS-TII), together with the NMR spectrum of this new polymer. Details on the synthesis and NMR characterizations of the TII monomer can be found in ESI.

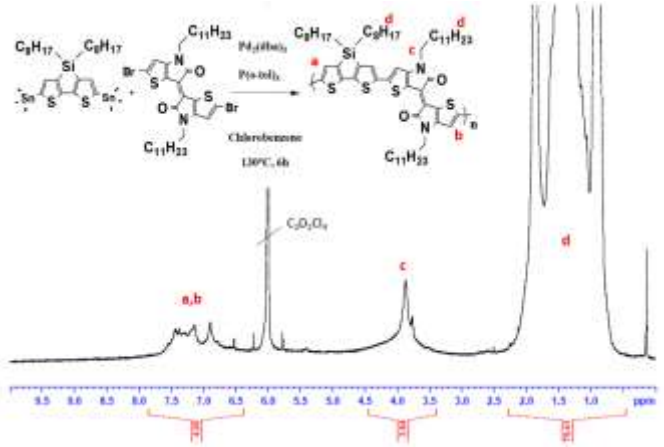

Figure 2: Stille cross-coupling polymerization using the stannilated DTS monomer with the dibrominated TII acceptor and $Pd_2(dba)_3$/$P(o\text{-}Tol)_3$ as the catalyst system in chlorobenzene, and NMR spectrum of P(DTS-TII). NMR data: 1H NMR (400 MHz, CDCl3) δ (ppm) = 7.7-6.7 (H aromatic, a and b, 4H/repetitive units), 3.8 (CH2-N, c, 4H/repetitive units), 2.1-0.5 (H aliphatic, d, 80H/repetitive units).

3. Results and discussion

3.1 Computational results

The parameters characterizing the ground-state geometries of the D-A monomers, namely the torsion angles θ around single bonds and the BLA along the conjugated skeleton, are reported in Table S1.1. Vertical transition energies and oscillator strengths, as well as the quantities characterizing the spatial extent of the charge transfer associated to the $S_0 \rightarrow S_1$ electronic transition ($\Delta\mu_{01}$, Δq and Δr), are collected in Table 1.

As it is typical for donor-acceptor π-conjugated systems, the $S_0 \rightarrow S_1$ transition is dominated by a π→π* electron excitation between the highest occupied and lowest unoccupied molecular orbital (HOMO and LUMO). The HOMO is delocalized on the whole molecule, whereas the LUMO is mainly localized on the electron-accepting moiety (see Table S1.2), which indicates that a significant intramolecular charge transfer (ICT) occurs between the D and A units upon light irradiation. As revealed by the data collected in Table 1, the absorption properties of D-A monomers are mostly driven by the nature of the acceptor, and remain quite insensitive to a change of donor. However, DTS-based derivatives are slightly blue shifted compared to those incorporating a CPDT or a DTP donor unit, mainly due to smaller energies of HOMOs (Table S1.2). For a given donor unit, adding a thiophene spacer between the D and A units from BT to DTBT redshifts the first absorption band by ~0.3 eV as a result of the extension of the conjugation length. Replacing the DTBT by a DPP unit shifts up the HOMO energy while the LUMO is downshifted, which translates into a lowering of the electronic and optical gaps, consistently with the decrease of the BLA. When moving from DPP to DAP, the substitution of the carbonyl groups by methylsulfanyl groups induces a large downshift of the LUMO while the HOMO energy hardly changes, which further

decreases the BLA and the transition energy towards the S_1 state. Finally, using TII as a withdrawing unit gives rise to BLA and $S_0 \rightarrow S_1$ transition energies similar to those calculated with A = DPP.

Table 1. Transition energies (ΔE_{01}, eV), oscillator strengths (f_{01}), charge transferred (Δq, |e|), charge transfer distance (Δr, Å) and dipole moment variation ($\Delta\mu_{01}$, D), calculated at the M06-2X/6-311G(d) level for the $S_0 \rightarrow S_1$ transition of the D-A monomeric units.

Monomer	ΔE_{01}	f_{01}	Δq	Δr	$\Delta\mu_{01}$
CPDT-BT	3.07	0.470	0.655	3.084	9.699
CPDT-DTBT	2.76	0.958	0606	2.932	8.538
CPDT-DPP	2.46	1.184	0.342	0.792	1.301
CPDT-DAP	2.18	1.125	0.381	2.308	4.223
CPDT-TII	2.36	0.698	0.436	1.651	3.453
DTS-BT	3.15	0.473	0.626	2.953	8.881
DTS-DTBT	2.78	0.996	0.590	2.650	7.513
DTS-DPP	2.47	1.175	0.336	0.498	0.804
DTS-DAP	2.19	1.103	0.493	0.344	0.815
DTS-TII	2.38	0.678	0.429	1.431	2.952
DTP-BT	3.08	0.447	0.693	3.211	10.682
DTP-DTBT	2.76	0.920	0.623	3.179	9.518
DTP-DPP	2.47	1.180	0.347	1.126	1.875
DTP-DAP	2.17	1.133	0.392	2.577	4.846
DTP-TII	2.37	0.679	0.446	1.839	3.944

Figure 3 further illustrates the electron density variation from the ground to the S_1 excited state in DTS-based D-A monomers, defined as $\Delta\rho = \rho_{S_1} - \rho_{S_0} = \Delta\rho^+ + \Delta\rho^-$, with $\Delta\rho^+$ ($\Delta\rho^-$) the areas where the density increases (decreases). Consistently with the fact that absorption properties mainly depend on the nature of the acceptor, the photo-induced ICT mainly spreads over the acceptor moiety and the thiophene spacer linking the D and A units, with the exception of BT (and to a lesser extent DTBT) where it partly extends onto the donor moiety. As a consequence, the dipole moment variation between the S_0 and S_1 states ($\Delta\mu_{01}$, Table 1) is much larger in derivatives incorporating these two donor groups, owing to larger amounts of charge transferred ($\Delta q \approx 0.6|e|$) as well as larger charge transfer distances ($\Delta r \approx 3$Å). On the other hand, the lowest ICT is obtained for DPP-based monomers, which also display the largest intensities of the $S_0 \rightarrow S_1$ absorption band, as indicated by the values of the associated oscillator strengths.

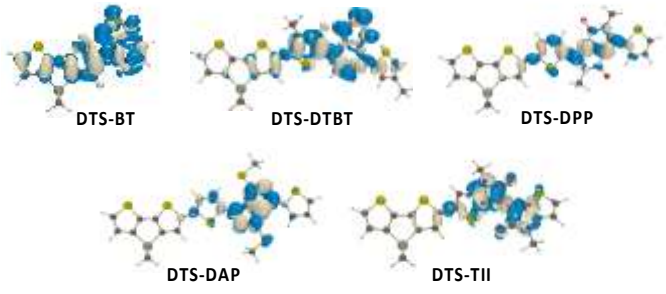

Figure 3: Electron density difference maps of DTS-based monomers, calculated at the M06-2X/6-311G(d) level. Blue (white) lobes are associated with positive (negative) $\Delta\rho$ values

The evolution of the lowest optical excitation energies of increasingly large oligomers (from n = 1 to n = 5 monomer units) as a function of the nature of the donor and acceptor units is illustrated in Figure 4, while numerical values are gathered in Tables S1.3-S1.7. Consistently with the decrease of the HOMO-LUMO gap, increasing the conjugated chain length induces a bathochromic shift of the main absorption band, up to a saturation limit that is reached for ~5 repeating units for all systems. Figure 4 clearly shows that the $S_0 \rightarrow S_1$ transition energy within a given oligomer series is mostly driven by the nature of the acceptor unit, whereas it remains quite insensitive to the nature of the donor moiety. This observation also holds true when considering the light harvesting properties of the various oligomers, as shown by the evolution with the oligomer size of the oscillator strengths per monomeric unit (Figure S1.4). Clearly, for a given number of repeating units, using a DAP acceptor moiety shifts the first absorption band to lower energies compared to the other withdrawing groups, and enhances the light harvesting capabilities of the oligomers.

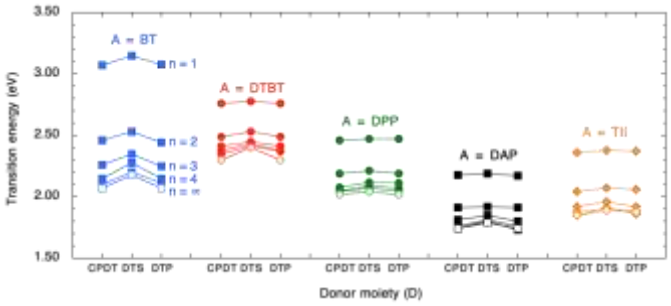

Figure 4: Evolution of the vertical transition energies of increasingly large oligomers (filled markers) as a function of the nature of the acceptor (A) and donor (D) moieties, as calculated at the M06-2X/6-311G(d) level. Empty markers correspond to extrapolations to infinite polymer chains

The transition energies in the polymer limit (ΔE_{01}^{∞}) evaluated using the fitting procedure based on the Kuhn's model, are reported as empty markers in Figure 4 (see also Figure S1.3 and Table S1.8). Consistently with the evolution of the absorption properties of finite size oligomers, the lowest excitation energies of polymers weakly depend on the nature of the donor group. Whatever the donor unit, the ΔE_{01}^{∞} values evolve in the following order depending on the nature of the associated acceptor: DAP < TII < DPP < BT < DTBT. This relative ordering is related to the evolution of the parameters of the Kuhn's model reported in Table S1.8. In particular, the absolute D_k value is decreasing from DAP to DTBT, revealing a decreasing efficiency of the electronic conjugation along the polymer backbone along the series.

Additional calculations performed for DTS-based derivatives accounting for solvent polarization effects (Table S1.9 and Figure S1.5) provided slightly lower ΔE_{01}^{∞} values without any change in their relative ordering (see Table 2). As a conclusion, DAP- and TII-based copolymers are expected to exhibit the lowest optical bandgaps within the investigated series. The computed values of oscillator strengths per monomeric unit (Figure S1.4) also indicate that, for a same polymer size, DAP-

based copolymers should display the highest efficiency in photon collection.

3.2 Experimental results

As shown in Figure 5 (top), the maximum absorption of DTS-based polymers measured in chloroform solutions covers the visible–NIR region from 580 nm P(DTS-DTBT) to 890 nm P(DTS-TII). In agreement with DFT calculations, adding thiophene spacers from P(DTS-BT) to P(DTS-DTBT) induces an hypsochromic shift of 0.12 eV of the main absorption band (Table 2). Then, redshifts towards the NIR region, together with a broadening of the first absorption band, are observed when varying the acceptor unit from DPP (0.59 eV), DAP (0.67 eV) to TII (0.75 eV). The band shifts measured as a function of the nature of the acceptor unit are in good agreement with DFT calculations, apart from the inversion between TII and DAP. This discrepancy might originate from the fact that solubilizing alkyl chains are not taken into account in calculations, neither the possible π–π stacking intermolecular interactions.

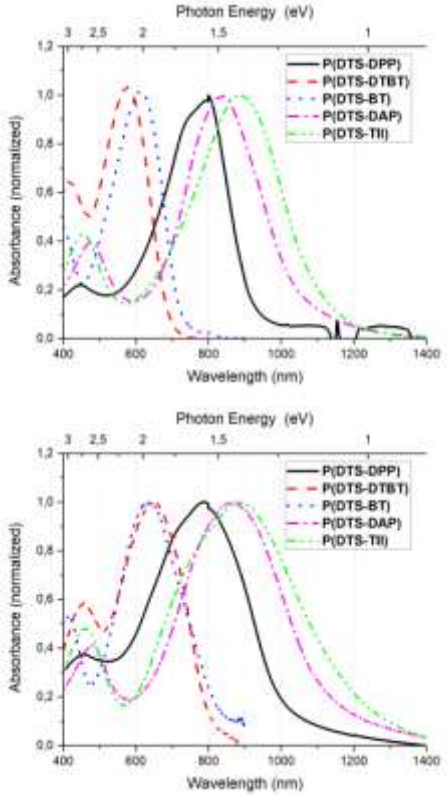

Figure 5: UV-visible spectra of DTS-based copolymers in chloroform solutions (top) and in thin films (bottom). Spectra are normalized to unity at the absorption maximum.

The optical properties of copolymers have been also studied in solid state, using thin films spin-coated from chloroform solutions and subsequently annealed at 140 °C for 15 minutes. Compared to measured spectra in solution, the films displayed broader absorption bands and exhibited a shoulder in the infrared region typical of intermolecular interactions in solid state (Figure 5, bottom).[41] The absorption edges (λ_{onset}) of the P(DTS-BT) and P(DTS-DTBT) films are about 800 nm, while for P(DTS-DPP), P(DTS-DAP) and P(DTS-TII) they are located in the second NIR window at 1010, 1120 and 1220 nm, respectively (Table 2). The optical bandgaps of the copolymer thin films, estimated according to $E_g^{opt}(eV) = 1240/\lambda_{onset}(nm)$, evolve in the same order depending on the nature of the acceptor as that measured in solution: TII < DAP < DPP < BT < DTBT.

The HOMO and LUMO levels deduced from cyclic voltammetry (Figure 6) are summarized in Table 2. Since all investigated copolymers involve a DTS unit as donor, the oxidation potentials are very close, with only 0.4 eV separating the highest lying HOMO level (-5.1 eV for P(DTS-TII)) from the deepest one (-5.5 eV for P(DTS-DPP)). As expected, the reduction potentials of the polymer films, which reflect the nature of the acceptor unit, span a broader range from -3.4 eV for P(DTS-BT) to -4.1 eV for P(DTS-DAP). In good agreement with DFT calculations (Tables S1.3-S1.7), the LUMO energies evolve in the following order with respect to the acceptor moiety: DAP < DPP < TII < DTBT < BT. Note that the copolymers containing the BT or DTBT acceptor unit display much higher LUMO energies than the three others, resulting in higher band gaps.

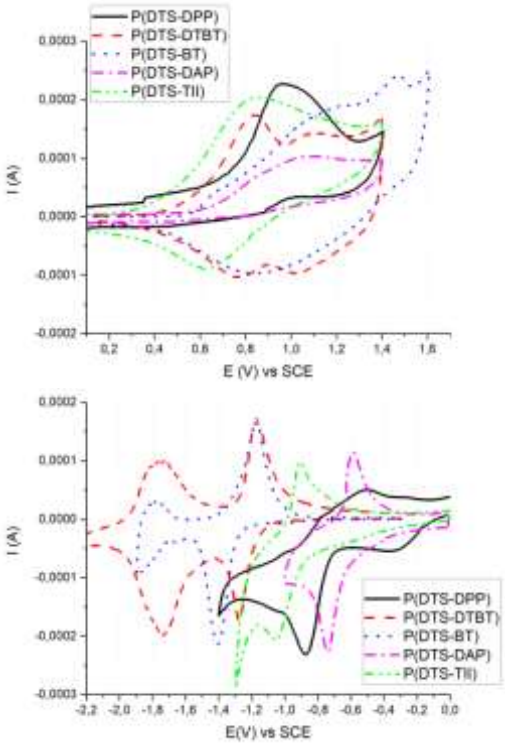

Figure 6: Cyclic voltammograms showing oxidation (top) and reduction (bottom) of copolymer films performed in 0.1 M Bu_4NPF_6/CH_3CN using a sweep rate of 0.1 $V.s^{-1}$.

Conclusions

This paper reports the synthesis and characterization of a new conjugated copolymer with alternating dithienosilole and

thienoisoindigo units. Joint experimental and computational characterizations provide detailed understanding of the absorption properties of this new system in comparison to a selection of 15 copolymers that combine benzothiadiazole, 4,7-di(thiophen-2-yl)-2,1,3-benzothiadiazole, diketopyrrolopyrrole and diazapentalene electron-withdrawing units to dithienosilole, cyclopentadithiophene or dithienopyrrole electron-donating units. DFT calculations carried out on increasingly large oligomers show that, within a given oligomer series, the energy of the first absorption band is mostly driven by the nature of the acceptor unit, while it is less sensitive to the nature of the donor moiety. DFT calculations also predict that the maximum absorption of copolymers including diazapentalene or thienoisoindigo electron-withdrawing units is redshifted compared to the other investigated systems, as a result of a better π−electron conjugation between the donor and acceptor moieties that is revealed by a lower bond length alternation along the conjugated backbone. Experimental characterizations confirmed that these two copolymers exhibit the most efficient absorption in the near-infrared region. In particular, the new dithienosilole-thienoisoindigo copolymer exhibits the largest absorption maximum wavelength in chloroform solution (890 nm) and largest absorption edges in both solution (1120 nm) and film (1220 nm). Its efficient near-infrared absorption suggests potential utility of this copolymer for optoelectronic applications such as photodetectors.

Table 2. Optical and Electrochemical Characteristics of the Synthesized Polymers.

Material	λ_{max} [a] (nm)	$E(\lambda_{max})$ (eV)	λ_{onset} [a] (nm)	E_g [a] (eV)	λ_{onset} [b] (nm)	E_g [b] (eV)	E_{HOMO} [c] (eV)	E_{LUMO} [c] (eV)	E_g [c] (eV)	ΔE_{01}^{∞} [d] (eV)
P(DTS-BT)	615	2.02	735	1.69	820	1.51	-5.3	-3.4	1.9	2.12
P(DTS-DTBT)	580	2.14	700	1.77	810	1.53	-5.3	-3.5	1.8	2.39
P(DTS-DPP)	800	1.55	920	1.35	1010	1.23	-5.5	-4.0	1.5	2.00
P(DTS-DAP)	840	1.47	1050	1.18	1120	1.11	-5.4	-4.1	1.3	1.67
P(DTS-TII)	890	1.39	1120	1.11	1220	1.02	-5.1	-3.8	1.3	1.80

[a] Measured by spectrophotometry in chloroform; [b] measured by spectrophotometry in film; [c] measured by cyclic voltammetry using E_{HOMO} (eV) = - (E_{ox} + 4.7) and E_{LUMO} (eV) = - (E_{red} + 4.7); [d] calculated at the IEF-PCM:M06-2X/6-311G(d) level in chloroform.

Conflicts of interest

There are no conflicts to declare.

Acknowledgements

The Agence Nationale de la Recherche (TAPIR project no. ANR-15-CE24-0024-02) and the Région Nouvelle Aquitaine (TAMANOIR project no. 2016-1R10105-0007207) are gratefully acknowledged for their financial support. Computer time was provided by the Pôle Modélisation HPC facilities of the Institut des Sciences Moléculaires, cofunded by the Nouvelle Aquitaine Région, as well as by the MCIA (Mésocentre de Calcul Intensif Aquitain) resources of the Université de Bordeaux and of the Université de Pau et des Pays de l'Adour.

Notes and references

1 J. Chen and Y. Cao *Acc. Chem. Res*. 2009, **42**, 1709.
2 P.-L. T. Boudreault, A. Najari, and M. Leclerc *Chem. Mater.* 2011, **23**, 456.
3 Y. Li *Acc. Chem. Res.* 2012, **45**, 723.
4 K. H. Hendriks, W. Li, M. M. Wienk and R. A. J. Janssen, *J. Am. Chem. Soc*. 2014, **136**, 12130.
5 W. Li, K. H. Hendriks, M. M. Wienk, and R. A. J. Janssen *Acc. Chem. Res.* 2016, **49**, 78.
6 L. Dou, Y. Liu, Z. Hong, G. Li, and Y. Yang *Chem. Rev*. 2015, **115**, 12633.
7 C. Liu, K. Wang, X. Gong and A. J. Heeger *Chem. Soc. Rev*. 2016, **45**, 4825.
8 J. Roncali *Chem. Rev*. 1997, **97**, 173.
9 Y. He, Y. Cao and Y. Wang, *Asian J. Org. Chem*. 2018, **7**, 2201.
10 Kenry, Y. Duan, B. Liu *Adv. Mater*. 2018, **30**, 1802394.
11 M. Li, L. Liu, C. Zhao, Y. Zhou, Y. Guo, J. Song, H. Wang *Dyes Pigm.* 2016, **134**, 480.
12 P. Cheng and X. Xhan *Chem. Soc. Rev*. 2016, **45**, 2544.
13 D. Tanaka, J. Ohshita, Y. Ooyama, Y. Morihara *Polym. J.* 2013, **45**, 1153.
14 Y. Adachi, Y. Ooyama, Y. Ren, X. Yin, F. Jäkle, J. Ohshita *Polym. Chem*. 2018, **9**, 291.
15 M. L. Keshtov, A. R. Khokhlov, S. A. Kuklin, A. Yu Nikolaev, E. N. Koukaras, G. D. Sharma *J. Polym. Sci. Part A: Polym. Chem*. 2018, **56**, 376.
16 T.Y. Chu, J. Lu, S. Beaupré, Y. Zhang, J.R. Pouliot, S. Wakim, J. Zhou, M. Leclerc, Z. Li, J. Ding, Y. Tao *J. Am. Chem. Soc.* 2011, **133**, 4250.
17 M. Zhang, X. Guo, Y. Li *Adv. Energy Mater*. 2011, **1**, 557.
18 L. Liao, L. Dai, A. Smith, M. Durstock, J. Lu, J. Ding, Y. Tao *Macromolecules* 2007, **40**, 9406.
19 J. Hou, H.Y. Chen, S. Zhang, G. Li, Y. Yang *J. Am. Chem. Soc.* 2008, **130**, 16144.
20 L. Huo, H.Y. Chen, J., Hou, T.L. Chen, Y. Yang *Chem. Commun*. 2009, **37**, 5570.
21 H. Medlej, H. Awada, M. Abbas, G. Wantz, A. Bousquet, E. Grelet, K. Hariri, T. Hamieh, R. C. Hiorns, C. Dagron-Lartigau, *Eur. Polym. J.* 2013, **49**, 4176.
22 S.-H. Kang, J. Lee, D. Yoo, B. H. Lee, C. Yang *J. Mater. Chem. C*, 2019, **7**, 8522.
23 W. Khelifi, H. Awada, K. Brymora, S. Blanc, L. Hirsch, F. Castet, A. Bousquet, C. Lartigau-Dagron *Macromolecules* 2019, **52**, 13, 4820.
24 R. S. Ashraf, A. J. Kronemeijer, D. I. James, H. Sirringhaus, I. McCulloch *Chem. Commun*., 2012, **48**, 3939.
25 G. W. Van Pruissen, F. Gholamrezaie, M. M. Wienk, R. A. Janssen, *J. Mater. Chem*., 2012, **22**, 20387
26 Y. Koizumi, M. Ide, A. Saeki, C. Vijayakumar, B. Balan, M. Kawamotoa, S. Seki *Polym. Chem.*, 2013, **4**, 484.
27 G. Kim, H. Kim, M. Jang, Y. Kyung Jung, J. Hak Oh, C. Yang *J. Mater. Chem. C*, 2016, **4**, 9554.
28 G.-Y. Chen, C.-M. Chiang, D. Kekuda, S.-C. Lan, C.-W. Chu, and K.-H. Wei *J. Polym. Sci. A Polym. Chem*., 2010, **48**, 1669.

29 Y. Zhang, J. Zou, C.-C. Cheuh, H.-L. Yip, and A. K.-Y. Jen, *Macromolecules* 2012 **45**, 5427.
30 J. Gierschner, J. Cornil, H. J. Egelhaaf, *Adv. Mater.* 2007, **19**, 173.
31 Y. Zhao, D. G. Truhlar *Theor. Chem. Acc*. 2008, **120**, 215.
32 M. Torrent-Sucarrat, S.; Navarro, F. P. Cossío, J. M. Anglada, J. M. Luis J. *Comput. Chem*. 2017, **38**, 2819.
33 A. Fradon, E. Cloutet, G. Hadziioannou, C. Brochon, F. Castet *Chem. Phys. Lett*. 2017, **678**, 9.
34 J. Tomasi, B. Mennucci, R. Cammi *Chem. Rev*. 2005, **105**, 2999.
35 W. Kuhn *Helv. Chim. Acta* 1948, **31**, 1780.
36 B. P. Karsten, L. Viani, J. Gierschner, J. Cornil, R. A. J. Janssen *J. Phys. Chem. A* 2008, **112**, 10764.
37 J. Torras, J. Casanovas, C. Alemán *J. Phys. Chem. A* 2012, **116**, 7571.
38 M. Wykes, B. Milián-Medina, J. Gierschner *Front. Chem*. 2013, **1**, 35.
39 E. F. Oliveira, J. C. Roldao, B. Milián-Medina, F. C. Lavarda, J. Gierschner *Chem. Phys. Lett*. 2016, **645**, 169.
40 M. J. Frisch, G. W. T., H. B. Schlegel, G. E. Scuseria, M. A. Robb, J. R. Cheeseman, G. Scalmani, V. Barone, B. Mennucci, G. A. Petersson, H. Nakatsuji, M. Caricato, X. Li, H. P. Hratchian, A. F. Izmaylov, J. Bloino, G. Zheng, J. L. Sonnenberg, M. Hada, M. Ehara, K. Toyota, R. Fukuda, J. Hasegawa, M. Ishida, T. Nakajima, Y. Honda, O. Kitao, H. Nakai, T. Vreven, J. A. Montgomery, Jr., J. E. Peralta, F. Ogliaro, M. Bearpark, J. J. Heyd, E. Brothers, K. N. Kudin, V. N. Staroverov, R. Kobayashi, J. Normand, K. Raghavachari, A. Rendell, J. C. Burant, S. S. Iyengar, J. Tomasi, M. Cossi, N. Rega, J. M. Millam, M. Klene, J. E. Knox, J. B. Cross, V. Bakken, C. Adamo, J. Jaramillo, R. Gomperts, R. E. Stratmann, O. Yazyev, A. J. Austin, R. Cammi, C. Pomelli, J. W. Ochterski, R. L. Martin, K. Morokuma, V. G. Zakrzewski, G. A. Voth, P. Salvador, J. J. Dannenberg, S. Dapprich, A. D. Daniels, Farkas, J. B. Foresman, J. V. Ortiz, J. Cioslowski and D. J. Fox, Gaussian 09 revision D01, Gaussian Inc. Wallingford CT 2009.
41 G. Li, V. Shrotriva, J. S. Huang, Y. Yao, T. Moriarty, K. Emery, Y. Yang, *Nat. Mater.* 2005, **4**, 864.
42